Electron-nuclear interaction in 13C nanotube double quantum dots

Churchill, H O H; Bestwick, A J; Harlow, J W; Kuemmeth, Ferdinand; Marcos, D; Stwertka, C H; Watson, S K; Marcus, C M

Published in:
Nature Physics

DOI:
doi:10.1038/nphys1247

Publication date:
2009

Document version
Publisher's PDF, also known as Version of record

nature physics

LETTERS

PUBLISHED ONLINE: 6 APRIL 2009 | DOI: 10.1038/NPHYS1247

Electron–nuclear interaction in ^{13}C nanotube double quantum dots

H. O. H. Churchill, A. J. Bestwick, J. W. Harlow, F. Kuemmeth, D. Marcos*, C. H. Stwertka, S. K. Watson* and C. M. Marcus†

For coherent electron spins, hyperfine coupling to nuclei in the host material can either be a dominant source of unwanted spin decoherence[1–3] or, if controlled effectively, a resource enabling storage and retrieval of quantum information[4–7]. To investigate the effect of a controllable nuclear environment on the evolution of confined electron spins, we have fabricated and measured gate-defined double quantum dots with integrated charge sensors made from single-walled carbon nanotubes with a variable concentration of ^{13}C (nuclear spin $I = 1/2$) among the majority zero-nuclear-spin ^{12}C atoms. We observe strong isotope effects in spin-blockaded transport, and from the magnetic field dependence estimate the hyperfine coupling in ^{13}C nanotubes to be of the order of 100 μeV, two orders of magnitude larger than anticipated[8,9]. ^{13}C-enhanced nanotubes are an interesting system for spin-based quantum information processing and memory: the ^{13}C nuclei differ from those in the substrate, are naturally confined to one dimension, lack quadrupolar coupling and have a readily controllable concentration from less than one to 10^5 per electron.

Techniques to prepare, manipulate and measure few-electron spin states in quantum dots have advanced considerably in recent years, with the leading progress in III–V semiconductor systems[2,3,10,11]. All stable isotopes of III–V semiconductors, such as GaAs, have non-zero nuclear spin, and the hyperfine coupling of electron spins to host nuclei is a dominant source of spin decoherence in these materials[1,2,12,13]. To eliminate this source of decoherence, group-IV semiconductors—various forms of carbon, silicon and silicon–germanium—which have predominantly zero nuclear spin, are being vigorously pursued as the basis of coherent spin electronic devices. Double quantum dots have recently been demonstrated in carbon nanotubes[14–16], including the investigation of spin effects[17,18].

The devices reported are based on single-walled carbon nanotubes grown by chemical vapour deposition using methane feedstock containing either 99% ^{13}C (denoted ^{13}C devices) or 99% ^{12}C (denoted ^{12}C devices; see the Methods section)[19]. The device design (Fig. 1a) uses two pairs of Pd contacts on the same nanotube; depletion by top-gates (blue, green and grey in Fig. 1a) forms a double dot between one pair of contacts and a single dot between the other. Devices are highly tunable, as demonstrated in Fig. 1, which shows that tuning the voltage on gate M (Fig. 1a) adjusts the tunnel rate between dots, enabling a crossover from large single-dot behaviour (Fig. 1b) to double-dot behaviour (Fig. 1c). Left and right tunnel barriers can be similarly tuned using the other gates shown in blue in Fig. 1a.

A notable feature of nanotube quantum dots that is not shared by GaAs dots is that the energy required to add each subsequent electron, the addition energy, often shows shell-filling structure even in the many-electron regime[18]. An example of a shell-filling pattern, with larger addition energy every fourth electron in the right dot, is seen in Fig. 1d. We find, however, that evident shell filling is not necessary to observe spin blockade at finite bias. Figure 2a,b shows current through the double dot, I_{dd}, as a function of gate voltages V_R and V_L for a weakly coupled, many-electron ^{13}C double dot at +1 and −1 mV source–drain bias, respectively, in a range of dot occupancy that does not show shell structure in the addition spectrum of either dot. With a magnetic field $B_{\|} = 200$ mT applied along the tube axis, current flow is observed throughout the finite-bias triangles at positive bias, but is suppressed at negative bias for detuning below 0.8 meV, which presumably indicates where an excited state of the right dot enters the transport window.

Current rectification of this type is a hallmark of spin blockade[10] (Fig. 2e): at positive bias, current flows freely as electrons of appropriate spin are drawn from the right lead to form the singlet ground state; at negative bias, current is blocked whenever a triplet state is formed between separated electrons, as the excess electron on the left can neither re-enter the left lead nor occupy the lowest orbital state on the right without flipping its spin. Spin blockade was identified in all four devices measured, two each of ^{12}C and ^{13}C. Spin blockade was occasionally found to follow a regular even–odd filling pattern, as seen in few-electron GaAs dots[20], although no pattern was seen adjacent to the area in Fig. 2.

Electrostatic sensing of the double-dot charge state is provided by a gate-defined quantum dot formed on a separately contacted portion of the same nanotube. The sensing dot is capacitively coupled to the double dot by a ∼1 μm coupling wire[21] (orange gate in Fig. 1a) but electrically isolated by a depletion gate between the Pd contacts. Charge sensor conductance g_s as a function of V_R and V_L, acquired simultaneously with transport data in Fig. 2a,b, is shown in Fig. 2c,d. The location of the coupling wire makes g_s sensitive to the occupancy of the right dot with no observable sensitivity to the left dot. Inside the positive-bias triangles (Fig. 2c), g_s is intermediate in value between their bordering regions, indicating that the excess electron is rapidly shuttling between the dots as current flows through the double dot. In contrast, inside the negative-bias triangles (Fig. 2d), g_s shows no excess electron on the right dot as a result of spin blockade.

The magnetic field dependence of spin blockade provides important information about electron spin relaxation mechanisms[22,23]. A first look at field dependence (Fig. 2f) for a ^{13}C device shows

Department of Physics, Harvard University, Cambridge, Massachusetts 02138, USA. *Present addresses: Departamento de Teoría de la Materia Condensada, Instituto de Ciencia de Materiales de Madrid, CSIC, Cantoblanco 28049, Madrid, Spain (D.M.); Department of Physics, Middlebury College, Middlebury, Vermont 05753, USA (S.K.W.). †e-mail: marcus@harvard.edu.

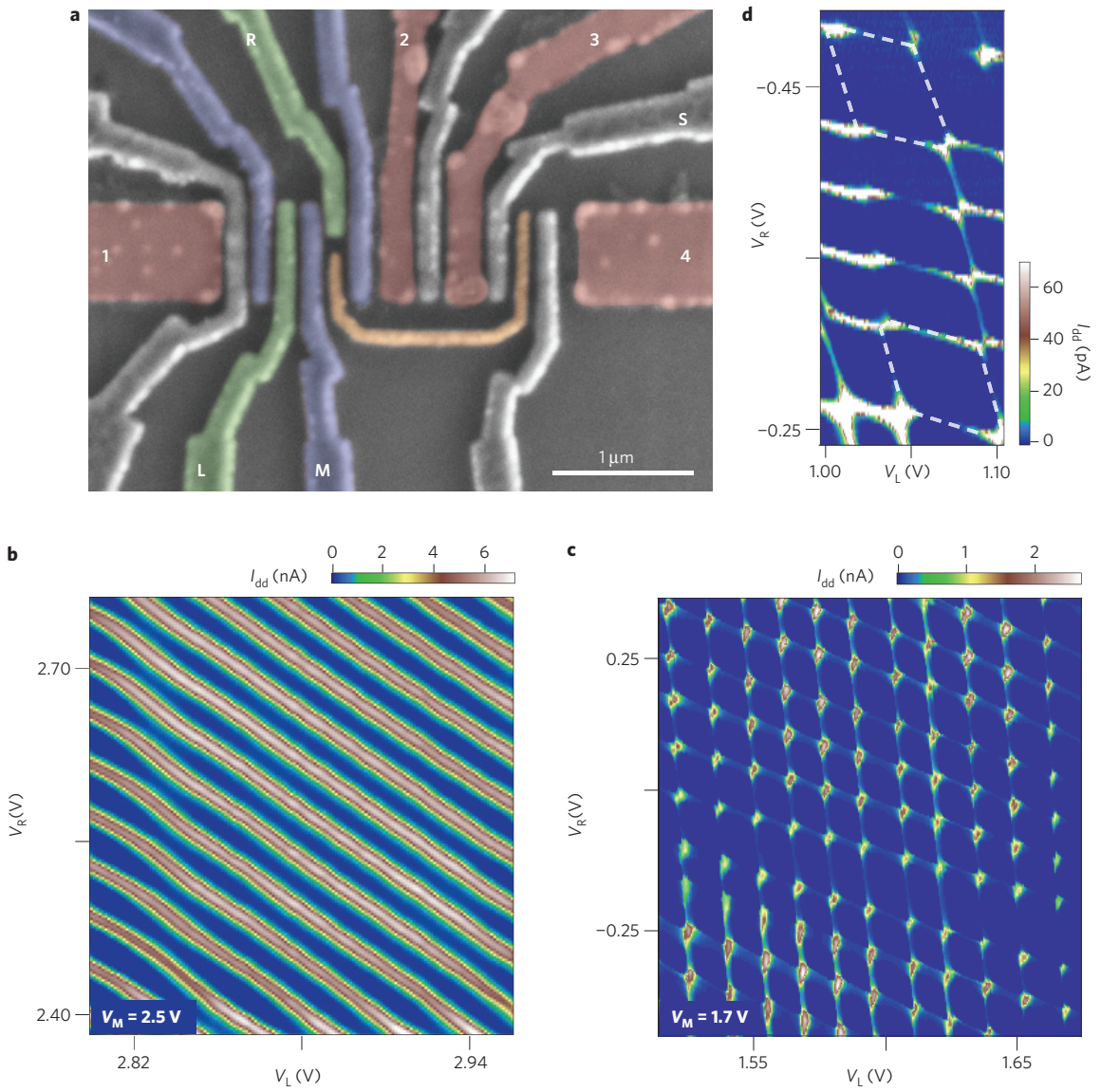

Figure 1 | Nanotube double dot with integrated charge sensor. a, Scanning electron micrograph (with false colour) of a device similar to the measured ^{12}C and ^{13}C devices. The carbon nanotube (not visible) runs horizontally under the four Pd contacts (red). Top-gates (blue) create voltage-tunable tunnel barriers enabling the formation of a single or double quantum dot between contacts 1 and 2. Plunger gates L and R (green) control the occupancy of the double dot. A separate single dot contacted by Pd contacts 3 and 4 is controlled with gate plunger gate S (grey) and is capacitively coupled to the double dot by a coupling wire (orange). **b**, Current through the double dot, I_{dd}, (colour scale) with the top-gates configured to form a large single dot. **c**, When carriers beneath the middle gate, M, are depleted, I_{dd} shows typical double-dot transport behaviour, demarcating the honeycomb charge stability pattern. **d**, Within certain gate voltage ranges, honeycomb cells with larger addition energy and fourfold periodicity (outlined with dashed lines) indicate the filling of spin and orbital states in shells. Source–drain bias is −1.0 mV for **b**–**d**.

that for negative bias (purple and green), spin-blockade leakage current is strongly peaked at $B_{\|} = 0$, whereas for positive bias (red), the unblockaded current does not depend on field. The peak in leakage current is shown for two values of V_M, indicating that the width of the peak is independent of interdot tunnel coupling t. As discussed below, this field dependence can be understood in terms of hyperfine-mediated spin relaxation.

The striking difference in field dependence of spin-blockade leakage current between ^{12}C and ^{13}C devices is illustrated in Fig. 3a,b. These data show that for negative (spin-blockaded) bias, leakage current is a minimum at $B_{\|} = 0$ for the ^{12}C device and a maximum at $B_{\|} = 0$ for the ^{13}C device. In fourteen instances of spin blockade measured in four devices (two ^{13}C and two ^{12}C), we find that leakage current minima can occur at $B_{\|} = 0$ in both ^{12}C and ^{13}C devices, particularly for stronger interdot tunnelling. For weak interdot tunnelling, however, only the ^{13}C devices show maxima of spin-blockade leakage at $B_{\|} = 0$, presumably because the width and height of this feature are strongly suppressed in ^{12}C nanotubes. In all cases, the positive bias (non-spin-blockade) current shows no appreciable field dependence.

Figure 3e shows spin-blockade leakage current as a function of $B_{\|}$ at fixed detuning (the detuning value is shown as a black line in Fig. 3a), along with a best-fit Lorentzian, for the ^{12}C device. The Lorentzian form was not motivated by theory, but seems to fit rather well. The width of the dip around $B_{\|} = 0$ decreases with decreasing interdot tunnelling (configuration Fig. 3e has $t \sim 50\,\mu$eV, on the basis of charge-state transition width[21]), which may explain why it is not observed in the weakly coupled regime of Fig. 3b,f. We note that a similar zero-field dip in spin-blockade leakage current was recently reported in a double dot formed in an InAs nanowire[24]. There the dip was attributed to spin–orbit coupling, an effect that is also present in carbon nanotubes[25].

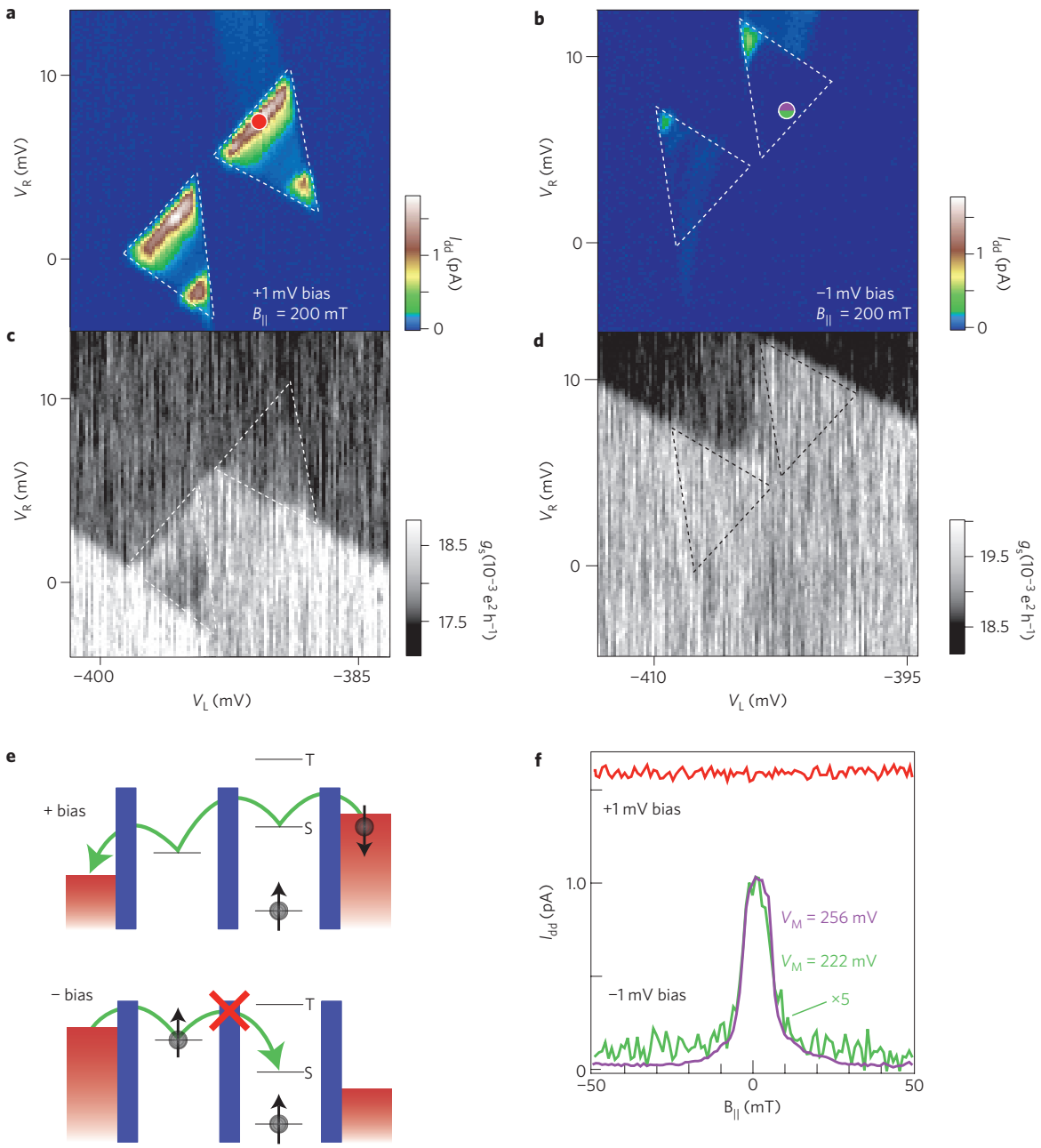

Figure 2 | Spin blockade in a ^{13}C nanotube double dot. a, Current I_{dd} (colour scale) at +1.0 mV source–drain bias, the non-spin-blockaded bias direction. Transport is dominated by resonant tunnelling through the ground state at the base of the finite-bias triangles and through an excited state at a detuning of 0.7 meV. **b**, I_{dd} (colour scale) at −1.0 mV source–drain bias, the spin-blockaded bias direction. I_{dd} is suppressed except near the tips of the transport triangles. Suppressed transport for one bias direction is the signature of spin blockade. **c**, Charge-sensing signal, g_s, (conductance of the sensing dot between contacts 3 and 4 in Fig. 1a), acquired simultaneously with **a** detects the time-averaged occupation of the right dot. **d**, Charge-sensing signal g_s for −1.0 mV bias (blockade direction). In **a**–**d**, dashed lines indicate allowed regions for current flow in the absence of blockade. **e**, Schematic diagram of spin-blockaded transport. Any spin may occupy the left dot, but only a spin singlet is allowed in the right dot, suppressing negative bias current once an electron enters the left dot and forms a triplet state. **f**, Current I_{dd} near zero detuning (position marked by circles in **a** and **b**) as a function of magnetic field for positive bias (non-blockade, red trace) and negative bias (blockade, for two values of V_M, purple and green traces). For $V_M = 222$, I_{dd} was multiplied by 5.

Hyperfine coupling appears to the confined electrons as an effective local Zeeman field (the Overhauser field) that fluctuates in time independently in the two dots, driven by thermal excitation of nuclear spins. The difference in local Overhauser fields in the two dots will induce rapid mixing of all two-electron spin states whenever the applied field is less than the typical difference in fluctuating Overhauser fields (at higher fields, only the $m = 0$ triplet can rapidly mix with the singlet). How hyperfine-mediated spin mixing translates to a field dependence of spin-blockade leakage current was investigated experimentally in GaAs devices[23], with theory developed by Jouravlev and Nazarov[22].

Field dependence of spin-blockade leakage current for a weakly coupled ^{13}C double dot near zero detuning is shown Fig. 3f, along with a theoretical fit (equation (11) of ref. 22, with a constant background current added), from which we extract a root mean square amplitude of fluctuations of the local Overhauser fields, $B_{nuc} = 6.1$ mT. We note that the width of the peak in Fig. 3f is independent of detuning (Fig. 3b), consistent with our

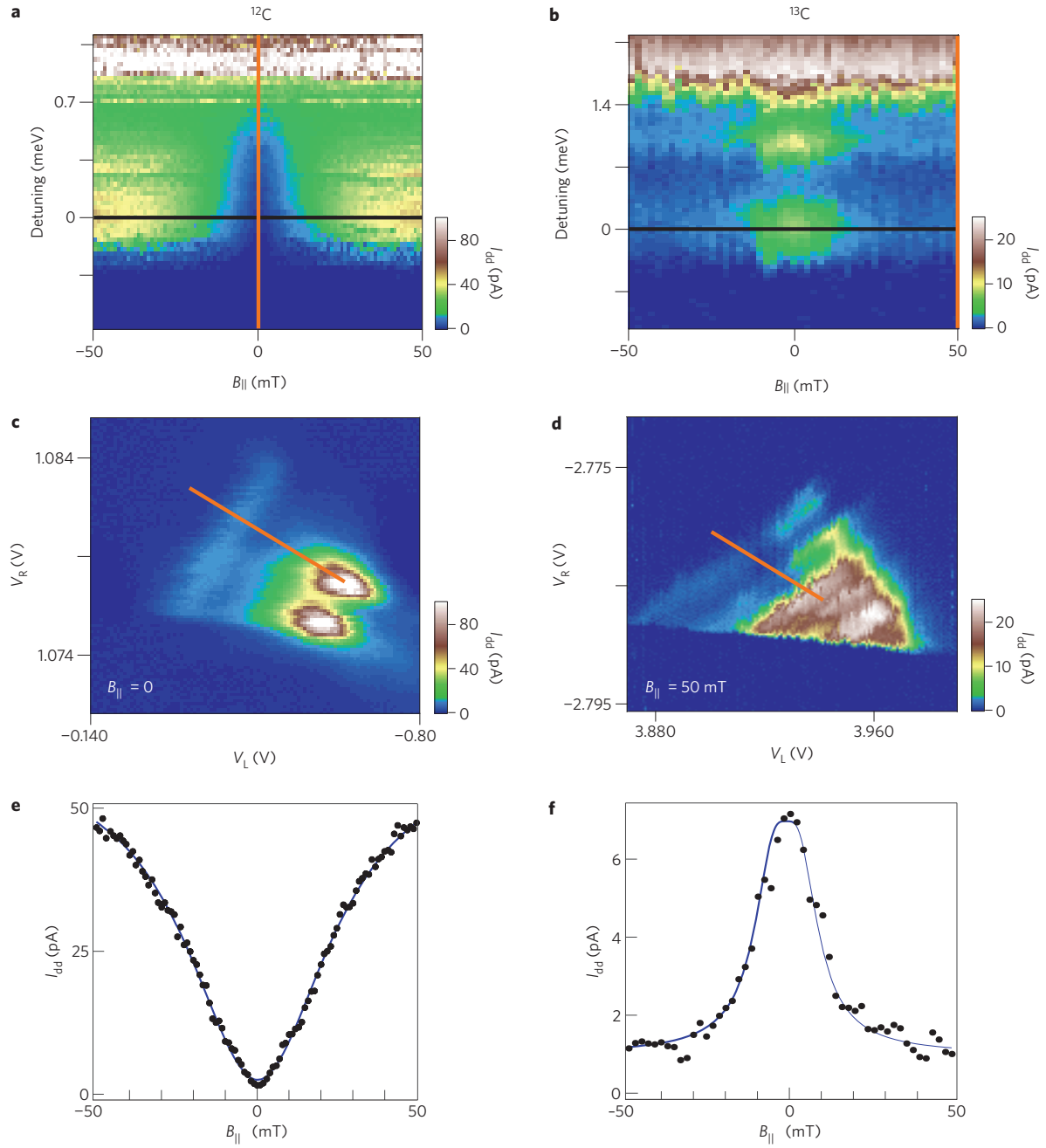

Figure 3 | Contrasting magnetic field dependence of leakage current for ^{12}C and ^{13}C devices. a,**b**, Leakage current through spin blockade (colour scale) as a function of detuning and magnetic field, $B_{||}$, for ^{12}C (**a**) and ^{13}C (**b**) devices. The vertical axes in **a** and **b** are interdot detuning as indicated by the orange lines in **c** and **d**, respectively. In **a**, $B_{||}$ was swept and detuning stepped, whereas in **b**, detuning was swept and $B_{||}$ stepped. **c**,**d**, Current through the double dot for a ^{12}C device (bias = −1.5 mV) and a ^{13}C device (bias = −4 mV), respectively. **e**,**f**, Cuts along $B_{||}$ at the detunings indicated by the black lines in **a** and **b**, respectively. The fit in **e** is a Lorentzian with a width of 30 mT, and the fit in **f** is to the theory of Jouravlev and Nazarov[22], providing a measure of $B_{nuc} = 6.1$ mT.

interpretation that it is governed by B_{nuc} rather than t. Assuming Gaussian-distributed Overhauser fields and uniform coupling, B_{nuc} is related to the hyperfine coupling constant A by $g\mu_B B_{nuc} = A/\sqrt{N}$, where g is the electron g-factor and N is the number of ^{13}C nuclei in each dot[22]. Taking $N \sim 3$–10×10^4 and $g = 2$ (see Supplementary Information), yields $A \sim 1$–2×10^{-4} eV, a value that is two orders of magnitude larger than predicted for carbon nanotubes[8] or measured in fullerenes[9].

Signatures of dynamic nuclear polarization provide further evidence of a strong hyperfine interaction in ^{13}C double dots. Hysteresis in the spin-blockade leakage current near zero detuning is observed when the magnetic field is swept over a tesla-scale range, as shown in Fig. 4a. The data in Fig. 4a,b are from the same ^{13}C device as in Fig. 3, but with the barriers tuned such that cotunnelling processes provide a significant contribution to the leakage current.

We interpret the hysteresis in Fig. 4a as resulting from a net nuclear polarization induced by the electron spin flips required to circumvent spin blockade[26]. We speculate that this nuclear polarization generates an Overhauser field felt by the electron spins that opposes $B_{||}$ once $B_{||}$ passes through zero. The value of the coercive field, $B_c \sim 0.6$ T, the external field at which

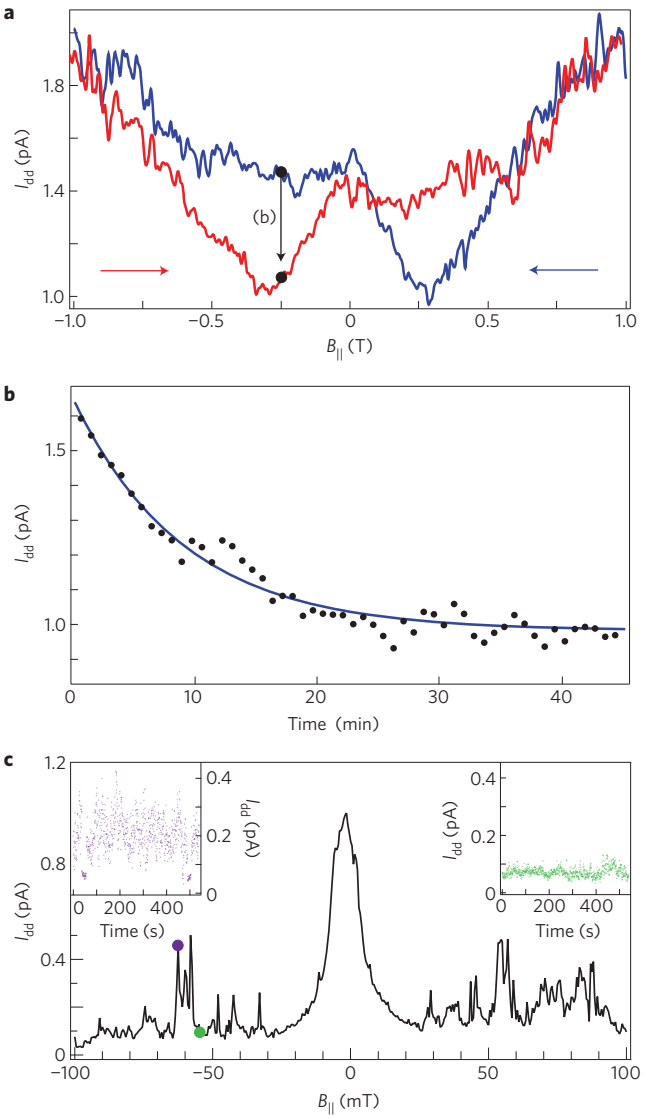

Figure 4 | Hysteresis and fluctuations in leakage current. a, The spin-blockade leakage current for a ^{13}C device measured for decreasing (increasing) magnetic field (sweep rate 0.4 mT s^{-1}), shown in blue (red), after waiting at +1 T (−1 T) for 10 min. A 2 mV source-drain bias is applied at all times. Hysteresis is seen on a field scale >0.5 T for both sweep directions. **b**, Decay of leakage current over time measured by stopping a downward sweep at −0.25 T (marked by a black arrow in **a**). The fit is to an exponential decay with a time constant of 9 min. **c**, Dependence of leakage current on $B_{||}$ near zero detuning in a second ^{13}C device. The leakage current fluctuates over time at some values of $B_{||}$, but remains steady at others (insets).

the two curves rejoin, places a lower bound for the hyperfine coefficient, $A \geq g\mu_B B_c \sim 0.7 \times 10^{-4}$ eV (equality corresponding to full polarization), independent of the value inferred from the width of the leakage current peak around zero field (Fig. 3f). If we instead use the value of A inferred from the current peak width (Fig. 3f), the size of B_c implies a ∼50% polarization for the data in Fig. 4a. Hysteresis is not observed for non-spin-blockaded transport in the ^{13}C devices and is not observed in the ^{12}C devices, suggesting that this effect cannot be attributed to sources such as the Fe catalyst particles or interaction with nuclei in the substrate or gate oxide.

Figure 4b shows that the induced nuclear polarization persists for ∼10 min, two orders of magnitude longer than similar processes in GaAs double dots[27]. The long relaxation time indicates that nuclear spin diffusion is extremely slow, owing both to the one-dimensional geometry of the nanotube and material mismatch between the nanotube and its surroundings. Field and occupancy dependence of relaxation were not measured.

Large fluctuations in I_{dd} are seen at some values of magnetic field, but not at others (Fig. 4c), similar to behaviour observed in GaAs devices[23]. This presumably reflects an instability in nuclear polarization that can arise when polarization or depolarization rates themselves are polarization dependent[26,28].

An important conclusion of this work is that the hyperfine coupling constant, $A \sim 1–2 \times 10^{-4}$ eV, in the ^{13}C devices (for both electron and holes, see the Methods section) seems to be larger than anticipated[8,9] and deserves further theoretical and experimental attention. It is possible that the substrate or gate oxide may enhance the degree of *s*-orbital content of conduction electrons, thus strengthening the contact hyperfine coupling. We also note that the one-dimensional character of charge carriers in ^{13}C nanotubes may greatly enhance the effective electron–nuclear interaction[29]. Finally, the large value of A motivates the fabrication of isotopically enriched ^{12}C nanotubes to reduce decoherence and the use of ^{13}C tubes as a potential basis of electrically addressable quantum memory.

Methods

Carbon nanotubes are grown by chemical vapour deposition using methane feedstock and 5-nm-thick Fe catalyst islands on degenerately doped Si substrates with 1 μm thermal oxide. ^{12}C devices are grown with methane containing natural abundance (1.1%) ^{13}C; ^{13}C devices are grown with 99% $^{13}CH_4$ (Sigma-Aldrich). Nanotubes are located after growth using a scanning electron microscope, and catalyst islands, source and drain electrodes (15 nm Pd) and top-gates (30 nm Al) are patterned using electron-beam lithography. After contacting with Pd, samples are coated with a non-covalent functionalization layer combining NO_2 and trimethylaluminium, followed by atomic layer deposition of a 30 nm Al_2O_3 top-gate insulator (Cambridge Nanotech Savannah atomic layer deposition system)[30]. Measurements were carried out in a dilution refrigerator with a base temperature of 30 mK and electron temperature of ∼120 mK, determined from the charge-sensing transition width[21]. The nanotubes presented in Figs 1 and 2 have small bandgaps ($E_g \sim 25$ meV); the ^{13}C nanotube in Fig. 3b,d,f and the other ^{12}C nanotube (data not shown) are large-gap semiconducting nanotubes. Charges occupying the dots and leads are electrons, except the data in Figs 3b,d,f and 4a,b, where the charge carriers are holes. No significant differences are seen between devices with electron and hole carriers.

Received 24 October 2008; accepted 4 March 2009; published online 6 April 2009

References

1. Khaetskii, A. V., Loss, D. & Glazman, L. Electron spin decoherence in quantum dots due to interaction with nuclei. *Phys. Rev. Lett.* **88**, 186802 (2002).
2. Petta, J. R. *et al.* Coherent manipulation of coupled electron spins in semiconductor quantum dots. *Science* **309**, 2180–2184 (2005).
3. Koppens, F. H. L. *et al.* Driven coherent oscillations of a single electron spin in a quantum dot. *Nature* **442**, 766–771 (2006).
4. Kane, B. E. A silicon-based nuclear spin quantum computer. *Nature* **393**, 133–137 (1998).
5. Taylor, J. M., Marcus, C. M. & Lukin, M. D. Long-lived memory for mesoscopic quantum bits. *Phys. Rev. Lett.* **90**, 206803 (2003).
6. Gurudev Dutt, M. V. *et al.* Quantum register based on individual electronics and nuclear spin qubits in diamond. *Science* **316**, 1312–1316 (2007).
7. Hanson, R., Dobrovitski, V. V., Feiguin, A. E., Gwyat, O. & Awschalom, D. D. Coherent dynamics of a single spin interacting with an adjustable spin bath. *Science* **320**, 352–355 (2008).
8. Yazyev, O. V. Hyperfine interactions in graphene and related carbon nanostructures. *Nano Lett.* **8**, 1011–1015 (2008).
9. Pennington, C. H. & Stenger, V. A. Nuclear magnetic resonance of C_{60} and fulleride superconductors. *Rev. Mod. Phys.* **68**, 855–910 (1996).
10. Ono, K., Austing, D. G., Tokura, Y. & Tarucha, S. Current rectification by Pauli exclusion in a weakly coupled double quantum dot system. *Science* **297**, 1313–1317 (2002).
11. Hanson, R. *et al.* Spins in few-electron quantum dots. *Rev. Mod. Phys.* **79**, 1217–1265 (2007).
12. Merkulov, I. A., Efros, Al. L. & Rosen, M. Electron spin relaxation by nuclei in semiconductor quantum dots. *Phys. Rev. B* **65**, 205309 (2002).
13. Coish, W. A., Fischer, J. & Loss, D. Exponential decay in a spin bath. *Phys. Rev. B* **77**, 125329 (2008).

14. Biercuk, M. J., Garaj, S., Mason, N., Chow, J. M. & Marcus, C. M. Gate-defined quantum dots on carbon nanotubes. *Nano Lett.* **5**, 1267–1271 (2005).
15. Sapmaz, S., Meyer, C., Beliczynski, P., Jarillo-Herrero, P. & Kouwenhoven, L. P. Excited state spectroscopy in carbon nanotube double quantum dots. *Nano Lett.* **6**, 1350–1355 (2006).
16. Gräber, M. R. *et al.* Molecular states in carbon nanotube double quantum dots. *Phys. Rev. B* **74**, 075427 (2006).
17. Buitelaar, M. R. *et al.* Pauli spin blockade in carbon nanotube double quantum dots. *Phys. Rev. B* **77**, 245439 (2008).
18. Jørgensen, H. I. *et al.* Singlet-triplet physics and shell filling in carbon nanotube double quantum dots. *Nature Phys.* **4**, 536–539 (2008).
19. Liu, L. & Fan, S. Isotope labeling of carbon nanotubes and formation of ^{12}C and ^{13}C nanotube junctions. *J. Am. Chem. Soc.* **123**, 11502–11503 (2001).
20. Johnson, A. C., Petta, J. R., Marcus, C. M., Hanson, M. P. & Gossard, A. C. Singlet-triplet spin blockade and charge sensing in a few-electron double quantum dot. *Phys. Rev. B* **72**, 165308 (2005).
21. Hu, Y. *et al.* A Ge/Si heterostructure nanowire-based double quantum dot with integrated charge sensor. *Nature Nanotech.* **2**, 622–625 (2007).
22. Jouravlev, O. N. & Nazarov, Y. V. Electron transport in a double quantum dot governed by a nuclear magnetic field. *Phys. Rev. Lett.* **96**, 176804 (2006).
23. Koppens, F. H. L. *et al.* Control and detection of singlet-triplet mixing in a random nuclear field. *Science* **309**, 1346–1350 (2005).
24. Pfund, A., Shorubalko, I., Ensslin, K. & Leturcq, R. Suppression of spin relaxation in an InAs nanowire double quantum dot. *Phys. Rev. Lett.* **99**, 036801 (2007).
25. Kuemmeth, F., Ilani, S., Ralph, D. C. & McEuen, P. L. Coupling of spin and orbital motion of electrons in carbon nanotubes. *Nature* **452**, 448–452 (2008).
26. Baugh, J., Kitamura, Y., Ono, K. & Tarucha, S. Large nuclear Overhauser fields detected in vertically coupled double quantum dots. *Phys. Rev. Lett.* **99**, 096804 (2007).
27. Reilly, D. J. *et al.* Exchange control of nuclear spin diffusion in a double quantum dot. Preprint at <http://arxiv.org/abs/0803.3082> (2008).
28. Rudner, M. S. & Levitov, L. S. Self-polarization and dynamical cooling of nuclear spins in double quantum dots. *Phys. Rev. Lett.* **99**, 036602 (2007).
29. Braunecker, B., Simon, P. & Loss, D. Nuclear magnetism and electronic order in ^{13}C nanotubes. Preprint at <http://arxiv.org/abs/0808.1685> (2008).
30. Farmer, D. B. & Gordon, R. G. Atomic layer deposition on suspended single-walled carbon nanotubes via gas-phase noncovalent functionalization. *Nano Lett.* **6**, 699–703 (2006).

Acknowledgements

We thank M. Biercuk, K. Flensberg, L. Kouwenhoven, D. Loss, E. Rashba and O. Yazyev for discussions, and D. Reilly for experimental assistance. This work was supported in part by the National Science Foundation under grant no. NIRT 0210736 and the NSF-NNIN Program, ARO/iARPA, the Department of Defense, Harvard's Center for Nanoscale Systems. H.O.H.C. acknowledges support from the NSF.

Additional information

Supplementary information accompanies this paper on www.nature.com/naturephysics. Reprints and permissions information is available online at http://npg.nature.com/reprintsandpermissions. Correspondence and requests for materials should be addressed to C.M.M.